Heliyon 9 (2023) e16067

Contents lists available at ScienceDirect

Heliyon

journal homepage: www.cell.com/heliyon

Research article

Green synthesis of highly efficient and stable copper oxide nanoparticles using an aqueous seed extract of Moringa stenopetala for sunlight-assisted catalytic degradation of Congo red and alizarin red s

Gemechu Fikadu Aaga [a,*], Sisay Tadesse Anshebo [b]

[a] College of Natural and Computational Sciences, Department of Chemistry, Dilla University, Dilla Ethiopia
[b] College of Natural and Computational Sciences, Department of Chemistry, Hawassa University, Hawassa Ethiopia

ARTICLE INFO

Keywords:
Copper oxide nanoparticles
Green synthesis
Alizarin red S
Congo red
Photocatalytic degradation
Kinetics study
Solar irradiation

ABSTRACT

Environmental pollution by organic pollutants because of population growth and industrial expansion is a global concern. Following this, the fabrication of single and efficient nanomaterials for pollution control is highly demanded. Under this study, highly efficient and stable copper oxide nanoparticles (CuO NPs) were synthesized through the green method using Moringa stenopetala seed extract. XRD, UV–vis, FT-IR, and SEM were applied to characterize the synthesized material. From XRD data, the average particle size was found to be 6.556 nm, and the nanoparticles are crystalline in nature. The formation of CuO NPs was demonstrated by FT-IR spectra of Cu–O in different bending vibration bands at 535 cm-1 and 1122 cm-1, as well as stretching vibration of Cu–O at 1640 cm-1. From UV–visible spectroscopic measurements, the energy band gap of greenly synthesized CuO NPs was found to be 1.73 eV. The SEM result shows that the nanoparticles' surfaces are rough, with some of the particles having spherically random orientation. The photodegradation efficiency of green synthesized CuO NPs photocatalyst was found to be 98.35% for Congo red at optimum experimental parameters (initial concentration, 25 mg/L; exposure time, 120 min; catalyst dose, 0.2 g; and pH, 5) and 95.4% for Alizarin Red S at optimum experimental parameters (catalyst dose, 0.25 g; initial concentration, 40 mg/L; exposure time, 120 min; and pH, 4.6). The COD values determined for the degraded product strongly support the complete mineralization of the dyes toward nontoxic materials. Reusability of the catalyst was investigated for five cycles, and the results clearly indicate the green synthesized CuO NPs are highly stable, can be used for several times, and are cost-effective as well. The degradation of Congo red and Alizarin red S on the surface of the CuO NPs follows the MBG kinetic model.

1. Introduction

Metal oxide nanoparticles are recently the most applicable material in the world especially in environmental pollution protection, in drug delivery, in battery cell, catalyst for synthesis, and antimicrobial activity [1–3]. Among those nanoparticles, CuO NPs is a

* Corresponding author.
E-mail address: gemechuf9@gmail.com (G.F. Aaga).

https://doi.org/10.1016/j.heliyon.2023.e16067
Received 27 February 2023; Received in revised form 28 April 2023; Accepted 4 May 2023
Available online 6 May 2023

p-type semiconductor of huge applications as it is cheap, stable and environmental friendly material [4]. CuO NPs has low band gap energy which makes it preferable material in photocatalytic reaction [5]. This material is recently the most applicable material in different areas, in batteries [6], electrochemical corrosion inhibition [7], photocatalytic reaction [8], antibacterial activity [9], and adsorption technology [10]. Usually it is prepared by mixing with another material to alter its performance and employed for different application [11].

On the other hand, environmental pollution by human action and natural phenomena is the one that needs attention because of the human health problem and other organisms caused by the pollution. These pollutants can be inorganic, Organic or organo-metallic in type and among them, persistent organic pollutants are absolutely toxic to human and other animals [12]. Organic dyes are a type of these persistent organic pollutants. Though these dyes are used in different industries such as textiles, cosmetics, leather tanning, paper, pharmaceutical, plastic and practical laboratories of schools, colleges, Universities and the others, they are highly toxic to human and other organisms if not properly managed and if they let out to the environment [13]. There were different techniques applied over the last decades like adsorption [14–20], flocculation [18,21], chemical oxidation [22], coagulation [23], and ion exchange method [24] for the removal of toxic organic pollutants. Not only these, for the treatment of polluted air and aqueous system different materials such as metal and metal oxide nanoparticles as well as MOF [25–27] were prepared and utilised. However, the above mentioned methods have their own limitations such as incomplete removal of the pollutant, a slow process, high energy consumption and material consumption, high cost, and production of secondary pollutants or large amount of sludge that require further disposal. Therefore, the photocatalytic degradation is a suitable choice for the degradation of POP because of its efficiency, simplicity and inability to generate secondary pollutant [28–30].

For the degradation of these organic dyes, metal oxides NPs are a good candidate as a photocatalyst [31]. The nanomaterials can be synthesized through green and chemical methods [7,32–35] and utilised for different purposes. In a chemical method, toxic and environmentally unfriendly chemicals or reducing agents such as hydrazine hydrate, sodium borohydride, dimethylformamide, ethylene glycol, and so on are commonly used [36]. Not only is their toxicity a problem, but these chemicals are expensive and not economic at all. As a result, an environmentally friendly, cost-effective, and fast production rate synthesis approach is required.

Therefore, this work aims at the green synthesis of copper oxide nanoparticles using Moringa stenopetala seed extract as a reducing and capping agent, their characterization, and their application for photocatalytic degradation of Congo red and alizarin red S dyes. In this work, green method is more preferred because of its advantage over the other methods. In green method, toxic chemicals are replaced by green reactants, high energy is not needed, cost of synthesis is reduced and large scale production can be easily employed [37,38]. CuO NPs are more preferable because of their low band gap energy, which makes it possible to use under sun light irradiation, their stability for reusability, and the fact that the copper salts are cheap, which makes it cost effective for wider application. To the best of our knowledge from our survey, CuO NPs were not prepared using *Moringa stenopetala* seed extract as reducing and capping agent. This plant belongs to the family of moringinaceae and is cultivated in Ethiopia specially in Gamo Gofa, Konso Wolayta and Sidama where the local people consume its leaves as part of their diet [39,40]. Many researchers used *Moringa stenopetala* leaf extract for synthesis of nanomaterials and also reported that its leaves contain different secondary metabolites. But the leaf this plant is consumed as food and is not recommended to be used for this purpose. For this reason and because its seed was reported to contain different secondary metabolites [41,42], i.e., glucosinolates, 5,5-dimethyloxazolidine-2-thione [43], isobutylthiocyanate and benzyl isothiocyanate [44], its seed extract was selected as a reducing and capping agent for the preparation of CuO NPs. Congo red and alizarin red S were selected as a representative organic dyes for evaluation of the degradation efficiency of CuO NPs. Moreover, in most

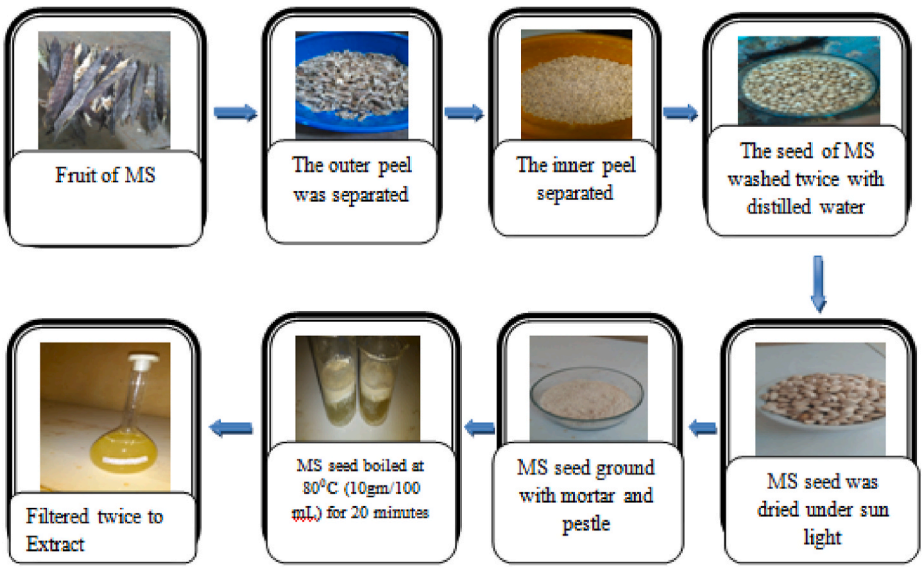

Fig. 1. Flow diagram for the preparation of *M. Stenopetala* seed extract.

of the early reported literature, the degradation of organic dyes occurs under UV irradiation with the support of hydrogen peroxide. But this approach is not safe at all, and because of this reason using sunlight as an energy source is safe, and it was used in this study.

2. Experimental section

2.1. Materials

All chemicals used were analytical grade. 95% of Cu $(NO_3)_2.3H_2O$ (LOBA CHEMIE) was used for the preparation of CuO nanoparticles as metal ion precursor. Congo red (SAMIR TECH-CHEM, LTD) and Alizarin red S (LOBA CHEMIE) dyes were used for the evaluation of photocatalytic activity of the prepared CuO nanoparticle. NaOH (Abron Experts-133 001, India) and 37% HCl (Sigma-Aldrich) were used for adjusting pH of the sample. Distilled water was used throughout the experiment for preparing solutions, plant extract and for washing purposes. Sulfuric acid, potassium dichromate (LOBA CHEMIE), ferrous ammonium sulfate (LOBA CHEMIE), silver sulfate, mercuric sulfate (Alpha chemika), and phenanthroline ferrous sulfate indicator were used to investigate the chemical oxygen demand of the final degraded product.

2.2. Preparation of Moringa stenopetala seed extract

For the preparation of seed extract (Fig. 1), mature and healthy Moringa stenopetala fruit was collected from land farms in Dilla, Gedeo Zone, Southern Nation, Nationality, and People's Region. Then the peel was separated from its seed, and the obtained seed was washed with tap water, then distilled water to remove dust, and dried under the shade. The dried seed was ground using a grinding machine, followed by packing in airtight glassware. The extraction was carried out by placing 10 g of powdered seed of Moringa stenopetala in a 250-mL conical flask containing 100 mL of distilled water and boiling at 80 °C for 20 min until the color changed to light brown. Then the plant extract was filtered twice using Whatman filter paper and stored in a refrigerator for the next application.

2.3. Green synthesis of copper oxide nanoparticles

The synthesis of CuO NPs was done according to the method on [45]. 20 mL of Moringa stenopetala aqueous extract was vigorously mixed with a homogeneous solution of copper metal precursor (0.1 M, 80 mL) for 4 h at 80 °C until a black colour was obtained, and then cooled to room temperature. Finally, the formed paste-like product was scratched and calcined in a muffle furnace at 400 °C for 2 h, yielding black-colored nanomaterial (Fig. 2).

2.4. Characterization

The crystalline structure and particle size of the synthesized CuO NPs were investigated by an X-ray diffractometer (Shimadzu XRD-7000S). The patterns were run with Cu-filtered CuKα radiation (λ = 1.54059 Å) energized at 40 kV and 15 mA. The samples were measured at room temperature in the range of 2θ = 10° to 60°. Functional group and chemical bond identification were analyzed by Spectrum 65 FT-IR spectrometer (PerkinElmer) for both CuO NPs and plant seed material with the scanning range of 4000 cm^{-1} to 400 cm^{-1}. Optical absorption and optical energy band gap measurements were carried out with a double-beam UV–Vis spectrophotometer

Fig. 2. Flow diagram of green Synthesis of CuO Nanoparticles. (For interpretation of the references to color in this figure legend, the reader is referred to the Web version of this article.)

(SM-1600 spectrophotometer). Scanning electron microscopy (JEOL/EO-JCM-6000 Plus) was taken to examine the morphology of the green route of CuO NPs.

2.5. Photocatalytic degradation experiment

To test the efficacy of the synthesized CuO NPs, 0.1 g of them were placed in a beaker with 50 mL of dye aqueous solutions. Prior to natural sunlight irradiation, a beaker containing the mixture of nanoparticles and dye solution was stirred for 30 min on a magnetic stirrer in the dark. This was done to keep the adsorption and desorption processes between dye molecules and the CuO NPs surface in balance. After 30 min, a beaker containing the dye solutions with nanoparticles was exposed to sunlight irradiation with the highest light intensity from 11:30 a.m. to 3:00 p.m.; the dye solutions with nanoparticles in the beaker were then centrifuged for 5 min at 1400 rpm using a centrifuge. The extent of the degradation was monitored by measuring the absorbance before and after degradation at 426 nm and 497 nm for Alizarin red S and Congo red, respectively. The effects of experimental parameters such as the initial concentration of the dyes, pH, exposure time, and photocatalyst dose were studied. The kinetics of the degradation was also investigated for both of the dyes. The chemical oxygen demand (COD) of the final product after degradation was investigated to evaluate the efficiency of greenly synthesized CuO NPs for effective degradation.

The COD in mg of O_2/L in a final degraded product was calculated using equation (1).

$$COD\left(\frac{mg}{L}\right) = \frac{8(V_{bl} - V_S) * M}{V} * 1000 \tag{1}$$

Where V_{bl} and V_s are volume of ferrous ammonium sulfate consumed for the blank and degraded product in mL, M is the molar concentration of the ferrous ammonium sulfate solution and V is the volume of the degraded product taken.

The reusability of the greenly synthesized CuO NPs was investigated just by recollecting the photocatalyzed CuO NPs through centrifugation. The nanoparticles were collected and washed twice with distilled water and then with ethanol before being used for degradation.

The percent of degradation was calculated by using equation (2).

$$Degradation\ percentage = \frac{A_0 - A_t}{A_0} * 100 \tag{2}$$

Where, A_0 is absorbance before degradation and A_t is absorbance of the dyes at a time t, on degradation.

2.6. Kinetics study

In the present study, three kinetics models have been tested in order to predict the photodegradation data of the dyes: the pseudo-zero-order, pseudo-first-order, and pseudo-second-order kinetics models. The photodegradation pseudo-kinetics experiments were carried out at different exposure times ranging from 30 to 120 min at 40 mg/L and 25 mg/L initial concentrations of Alizarin red S and Congo red, respectively. During this work, all other experimental parameters were optimized while being kept constant. This kinetics study was investigated by using the linearized equation for zero-order kinetics, first-order kinetics, second-order kinetics and BMG model as shown on equations (3)–(6), respectively.

$$C_0 - C = k_0 t \tag{3}$$

$$\ln\left(\frac{C_0}{C}\right) = k_1 t \tag{4}$$

$$\frac{1}{C} - \frac{1}{C_0} = k_2 t \tag{5}$$

$$\frac{t}{1 - \frac{C}{C_o}} = \frac{t}{m} \tag{6}$$

Where C_o is initial concentration of the dyes, C is concentration of the dyes at time t, k is the rate constant and t is time.

3. Result and discussion

3.1. Characterization

3.1.1. X-ray diffraction (XRD) analysis

X-ray diffraction was used to examine the phase purity and crystallinity of green-route synthesized CuO NPs (Fig. 3). The XRD analysis of Moringa stenopetala seed extract-mediated greenly synthesized CuO NPs has confirmed the crystalline structure of the nanoparticle. Fig. 3 shows typical XRD pattern of green synthesized CuO NPs diffraction peaks at 2 θ of 32.22°, 35.42°, 38.64°, 48.60° and 58.02°, and these diffraction peaks were matched to (1 1 0), (0 0 2), (1 1 1), (2 0 2), and (2 0 2) CuO NPs. These diffraction peaks

agree well with JCPDS card 89–2529, confirming that the CuO NPs synthesized are crystalline and monoclinic in structure [45]. The average particle size of the nanoparticle is calculated by the Debye-Scherrer equation, as shown in equation (7):

$$D = \frac{k\lambda}{\beta \cos\theta} \tag{7}$$

where D is the average crystalline size, K is the Scherrer constant (usually 0.9), is the X-ray source's wave length, Cu k radiation (1.5406), is the diffraction's full width at half maximum (FWHM) in radians, and is Bragg's diffraction angle, and it was found to be 6.556 nm.

3.1.2. Fourier transform infrared spectroscopy (FT-IR) analysis

Fig. 4A and B shows the FT-IR spectra of Moringa stenopetala seed powder and the green synthesized CuO NPs, respectively. The peaks at 2920 cm^{-1} and 3389 cm^{-1} belong to the symmetric and asymmetric stretching vibrations of the O–H bond, respectively, and may be because of absorbed moisture. The presence of bands at 535 cm^{-1} and 1122 cm^{-1} indicates different modes of bending vibration of the Cu–O bond. The appearance of the peak at 1640 cm^{-1} indicates that the Cu–O bond of copper (II) oxide nanoparticles is stretching [46]. This FT-IR spectrum strongly suggests the formation of the desired CuO NPs. On the FT-IR spectrum of the seed powder of the plant, the broad peak at 3316 cm^{-1} belongs to the O–H stretching vibration of the water molecule. The absorption peaks at 2924 cm^{-1} and 2856 cm^{-1} were identified as asymmetric and symmetric C–H stretching vibrations of aliphatic groups; the peak at 1750 cm^{-1} is because of C–O stretching carbonyl; the peak at 1652 cm^{-1} is because of N–H stretching vibrations of amine molecules; the peak at 1466 cm^{-1} was attributed to C–N stretching vibration, the peak at 1163 cm^{-1} to C–O stretching, and the peak at 634 cm^{-1} to the N–H bending vibration. The peaks at 3316 cm^{-1}, due to O–H stretching of hydroxyl groups, and the peak at 1750 cm^{-1}, attributed to C═O stretching of carbonyl groups present in the seed extract, were approximated as the reducing agents in the green synthesis of CuO NPs.

3.1.3. Ultraviolet–visible spectroscopy analysis

Greenly synthesized CuO NPs' optical properties were investigated by measuring their absorbance in the 200–800 nm wavelength range and then calculating their band gap energy. The sharp absorbance peak at 280 nm of greenly synthesized CuO NPs confirmed the particles' nanoscale size (Fig. 5A). Moreover, this absorbance spectrum of CuO NPs is well associated with the previous report [45,47]. The energy band gap and transition type can be determined from the analysis of data obtained from optical absorbance versus wavelength with the Stern (1963) relationship of near edge-absorption, which is given in equation (8) [48]:

$$A = \frac{[k(h\nu - Eg)]^{\frac{n}{2}}}{h\nu} \tag{8}$$

Where A is absorbance, hν is the incident photon energy, k is a constant, and the exponent ''n'' assumes the values 1, 4, 3 and 6 for allowed direct, allowed indirect, forbidden direct and forbidden indirect transitions respectively. The energy band gap of the synthesized nanoparticles was obtained by extrapolating the linear portion of $(Ah\nu)^2$ versus Eg to the axis at $(Ah\nu)^2 = 0$, which is a straight line in the domain of higher energies, which indicates a direct optical transition. The energy band gap of the green synthesized CuO NPs obtained through extrapolation is 1.73 eV (Fig. 5B). This energy band gap is appropriate band gap energy as it is comparable with energy that can be obtained from solar radiation (sun light) and nearly similar with the previous report [49].

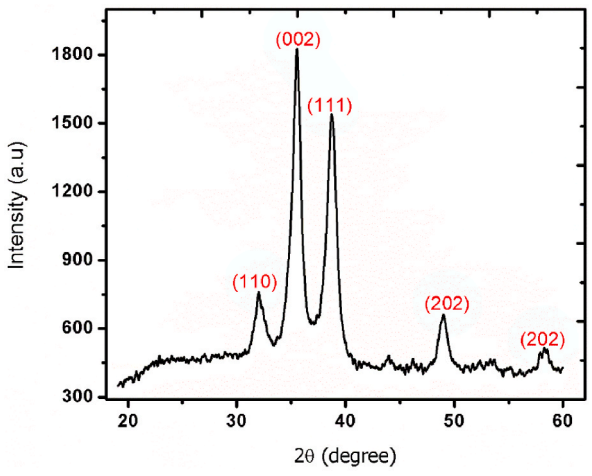

Fig. 3. XRD plot of green synthesized CuO NPs. (For interpretation of the references to color in this figure legend, the reader is referred to the Web version of this article.)

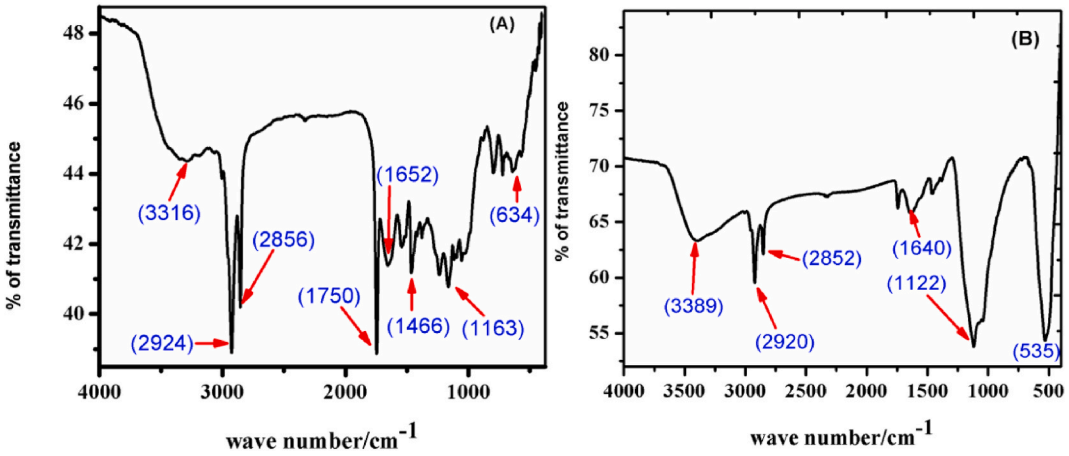

Fig. 4. FT-IR spectrum (A), moringa stenopetala seed and (B), green synthesized CuO NPs. (For interpretation of the references to color in this figure legend, the reader is referred to the Web version of this article.)

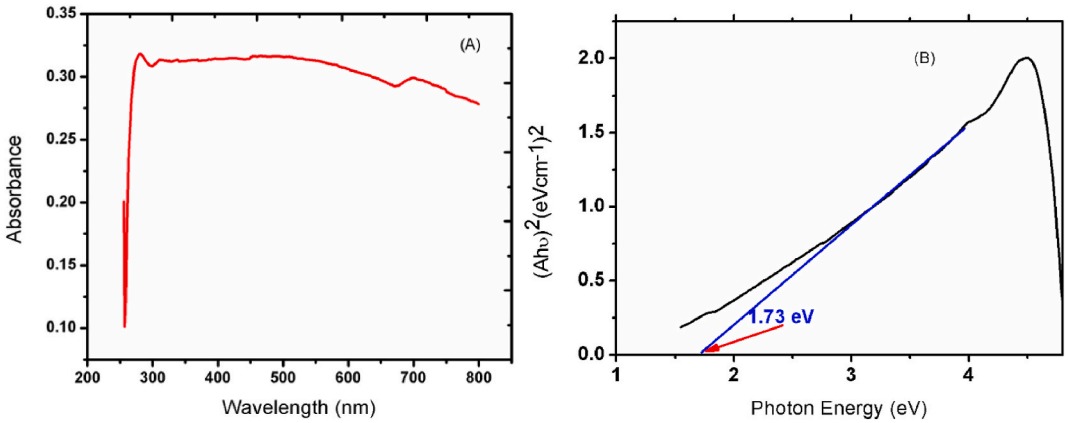

Fig. 5. UV–vis spectrum of (A), green synthesized CuO NPs and (B), $(Ah\nu)^2$ plotted as a function of energy ($h\nu$) for synthesized CuO NPs. (For interpretation of the references to color in this figure legend, the reader is referred to the Web version of this article.)

3.1.4. Scanning electron microscope (SEM) analysis

The SEM images for the green synthesized CuO NPs are shown on Fig. 6A and B. The images clearly show that the particles have a rough surface and some of them have a spherically random orientation. The analysis was done at two different magnifications, which were aimed at observing the morphology of the CuO NPs clearly.

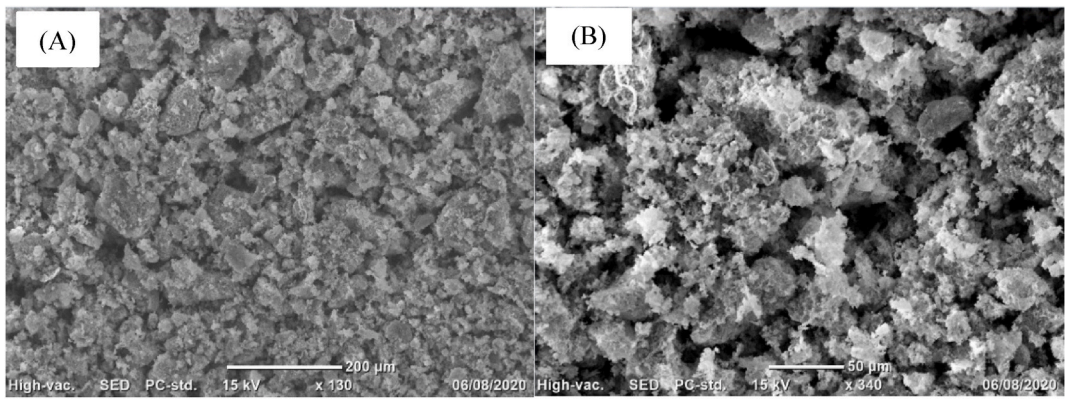

Fig. 6. SEM images of green synthesized CuO NPs at 200 μm and 50 μm.

3.2. Evaluation of photocatalytic activity of green synthesized CuO nanoparticles

The degradation of the selected organic dyes using CuO NP was studied by determining the optimum experimental parameters such as pH, initial dye concentration, catalyst dose, and exposure time. Observation of the decay in color and calculation of the percentage of degradation using the absorbance value before and after degradation were implemented as the preliminary screening of the occurrence of the degradation.

3.2.1. Effect of photo catalyst dose

Fig. 7 indicates the optimum dose of the prepared photocatalyst for the degradation of both dyes. For alizarin red S, degradation efficiency increased up to a dose of 0.25 g (94.78%) and then decreased. Also, the degradation efficiency of Congo red increases up to a catalyst dose of 0.2 g (92.7%). Lowering the catalyst dose below the optimum value reduces degradation because more light passes through the reaction medium and is used in the photocatalytic reaction [50].

This increase in degradation efficiency is due to the generation of more active sites on the photocatalysts surface as the dose of catalyst increases which consequently increases the number of hydroxyl and superoxide radicals. It has been reported that in heterogeneous photocatalytic reactions, the photo degradation of dye is in proportion with the loaded catalyst and it increases as a result of an increase in the amount of loaded catalyst [51]. As the catalyst dose increased further, the percent of degradation decreased due to light penetration inhibition, and less hydroxyl radical was generated. Aggregation of nanoparticles at high catalyst doses may also contribute to a lower degradation percentage by reducing the number of active sites and producing fewer active radicals [52,53].

3.2.2. Effect of initial concentration of the dyes

The optimization of the initial dye concentrations was performed by varying the initial dye concentrations (10 mg/L to 40 mg/L for Congo red with a gap of 5 mg/L and 10 mg/L to 70 mg/L for Alizarin red S with a gap of 10 mg/L) as presented in Fig. 8. The degradation efficiency increases up to 25 for Congo red, whereas for Alizarin red S, it increases up to 40 mg/L. Then, after these two optimum values of initial concentrations, the efficiency decreased. The increment in degradation with increasing the initial dye concentration is just because more dyes are available for degradation, and this will be true up to the optimum point. This decrease in degradation efficiency with increasing initial dye concentration above the optimum value is primarily due to a large amount of adsorbed dye, which may also inhibit reactions between dye molecules and reactive radicals [54]. Since the excessive dye concentration may hinder light penetration into the solution, fewer photons can reach the photocatalyst surface [55].

3.2.3. Exposure time

The effect of exposure time on the photodegradation of both dyes was investigated for both dyes and shown in Fig. 9. The degradation efficiency of both Congo red and Alizarin red S sharply increases up to 120 min and then seems to maintain constant efficiency above 120 min. This result indicates the time required for the degradation of the dyes within the efficiency of the prepared photocatalyst. When the time of total degradation of the dyes reached the degradation efficiency of the photocatalyst, further exposition time would not be useful as it couldn't bring more results beyond the efficiency of the catalyst.

3.2.4. Effect of pH

The optimum pH for both of the dyes was investigated and summarized in Fig. 10. The pH at which maximum degradation efficiency (95.4%) was obtained for Alizarin red S was 4.6 (the pH of the mixture of the dye and catalyst itself). The maximum degradation efficiency obtained at this pH is attributed to the effects of the pH in facilitating the adsorption between the dyes and the

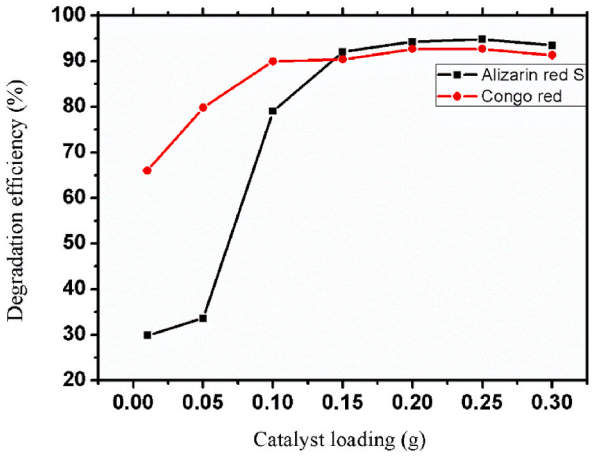

Fig. 7. Effect of catalyst loading on Alizarin red S and Congo red degradation with 10 mg/L/50 mL of Congo red and 30 mg/L/50 mL of Alizarin red S. (For interpretation of the references to color in this figure legend, the reader is referred to the Web version of this article.)

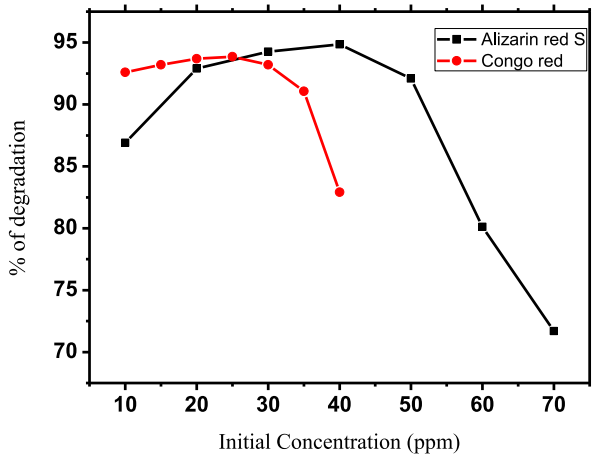

Fig. 8. Effect of initial concentration on Alizarin red S and Congo red degradation, catalyst dose: 0.25 g/50 mL for Alizarin red S and 0.2 g/50 mL for Congo red. (For interpretation of the references to color in this figure legend, the reader is referred to the Web version of this article.)

photocatalysts. The optimum pH value for the degradation of Congo red was 5. This congo-red molecule is also an anionic dye (two negatively charged sulphonate groups per molecule). The high degradation percent at pH 5 (98.35%) is due to the possible adsorption between the dye and the catalyst. In this acidic medium, the catalyst is positively charged through protonation, and for both of the dyes, adsorption is possible here because of the electrostatic force of attraction between the dyes and the catalyst. This decrease in degradation efficiency above the optimum pH is mainly due to the electrostatic repulsion between the negatively charged group of the dyes and the negatively charged surface of the catalyst through the addition of the base [56].

At the optimum experimental parameters, the degraded products were taken, and their COD values were determined to be 16 mg/L and 19 mg/L for Congo red and alixarin red S, respectively. These COD values indicate that the greenly synthesized CuO NPs have good potential to effectively degrade the dyes and mineralize them into a nontoxic product.

A mechanism for degradation was proposed and presented in Fig. 11. When the mixture of CuO NPs and dyes is exposed to sunlight, the electron will excite in the conduction band, leaving a positive hole in the valence band. Then the exiting electron will be trapped by surface oxygen and produce hydroxyl radicals through photooxidation, whereas the positive charge will oxidize water to form hydroxyl radicals. The formed hydroxyl radical will degrade the dyes, forming non-toxic products such as CO_2 and H_2O.

The reusability of green-synthesized CuO NPs for photocatalytic degradation of both dyes demonstrates the nanoparticles' excellent performance. The regenerated CuO NPs showed good catalytic performance up to the fourth cycle and somewhat decreased on the fifth cycle (Fig. 12). This can be due to the loss of nanoparticles during washing. Therefore, the nanoparticles can be regenerated and used for degradation dyes under sunlight irradiation. The stability of greenly synthesized CuO NPs at optimum pH can also be observed from this recyclability study. Unless the nanoparticles are stable at the optimum pH, they cannot be used for degradation more than several times.

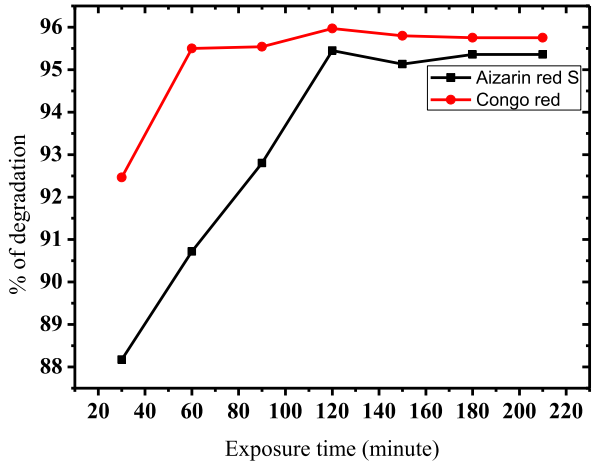

Fig. 9. Effects of exposition time for degradation of Alizarin red S and Congo red, Catalyst dose: 0.25 g/50 mL for Alizarin red S and 0.2 g/50 mL for Congo red, Initial concentration; 25 mg/L for congo red and 40 mg/L for Alizarin re S. (For interpretation of the references to color in this figure legend, the reader is referred to the Web version of this article.)

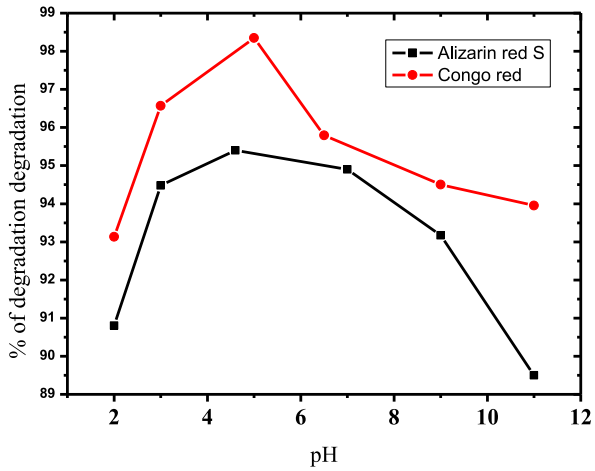

Fig. 10. Effect of pH for degradation of Alizarin red S and Congo red, Catalyst dose: 0.25 g/50 mL for Alizarin red S and 0.2 g/50 mL for Congo red, initial concentration; 25 mg/L for congo red and 40 mg/L for Alizarin re S, Contact time 120 min. (For interpretation of the references to color in this figure legend, the reader is referred to the Web version of this article.)

The comparison of the newly prepared CuO NPs with the previously reported green synthesized CuO NPs in terms of particle size and photocatalytic performance was reviewed and accumulated in Table 1. The summary shows that the greenly synthesized CuO NPs by using Moringa stenopetala seed extract as a reducing and capping agent have excellent performance in photocatalytic properties as well as an average particle size that is relatively small.

3.3. Kinetics study

The kinetics data for zero order (Fig. 13A), first order (Fig. 13B), second order (Fig. 13C), and the BMG model (Fig. 13D) were investigated. The degradation rate constant and correlation coefficient for each kinetic are calculated and summarized in Table 2. The data indicate that a correlation coefficient of 0.99999 and 0.9991 was obtained for Congo red and Alizarin red S on the BMG kinetic model. These values indicate that the degradation of Congo red and Alizarin red S on the surface of CuO NPs photocatalyst well fits the MBG kinetic model.

4. Conclusion

Under this study, highly efficient and stable copper oxide NPs were successfully synthesized by a green synthetic pathway and applied for photocatalytic degradation of Congo red and Alizarin red S. The characterization of CuO NPs was done by different analytical techniques such as XRD, FT-IR, UV–Visible, and SEM. XRD data confirmed green synthesized CuO NPs is crystalline in nature and that it is at a nano level (i.e 6.556 nm). FT-IR spectra revealed characteristic peaks of Cu–O bonds and functional groups present in seed extracts that are assumed as reducing and capping agents in the preparation of CuO NPs. Furthermore, from the UV–visible spectra of synthesized CuO NPs, an energy band gap was obtained. The nanoparticles have a bandgap energy of 1.73 eV. These all confirm the formation of the desired CuO NPs. From the photocatalytic degradation study, it is possible to conclude that these green-route synthesized CuO NPs have the efficacy to degrade Congo red and Alizarin red S under natural sunlight irradiation. The photocatalytic degradation was found to be strongly dependent on the photocatalyst dose, exposure time, pH, and the initial dye concentration. In the degradation of both of the dyes, maximum degradation efficiency was found to be 98.35% and 95.4% for Congo red and Alizarin red S respectively under optimum conditions. The kinetics study indicates that photocatalytic degradation of Alizarin red S and Congo red follows the BMG kinetic model. In general, CuO NPs can be applied for the treatment of organic dye-polluted aqueous solutions.

Declarations

Author contribution statement

Gemechu Fikadu Aaga: Conceived and designed the experiments; Performed the experiments; Analyzed and interpreted the data; Contributed reagents, materials, analysis tools or data; Wrote the paper.

Sisay Tadesse Anshebo: Conceived and designed the experiments; Analyzed and interpreted the data.

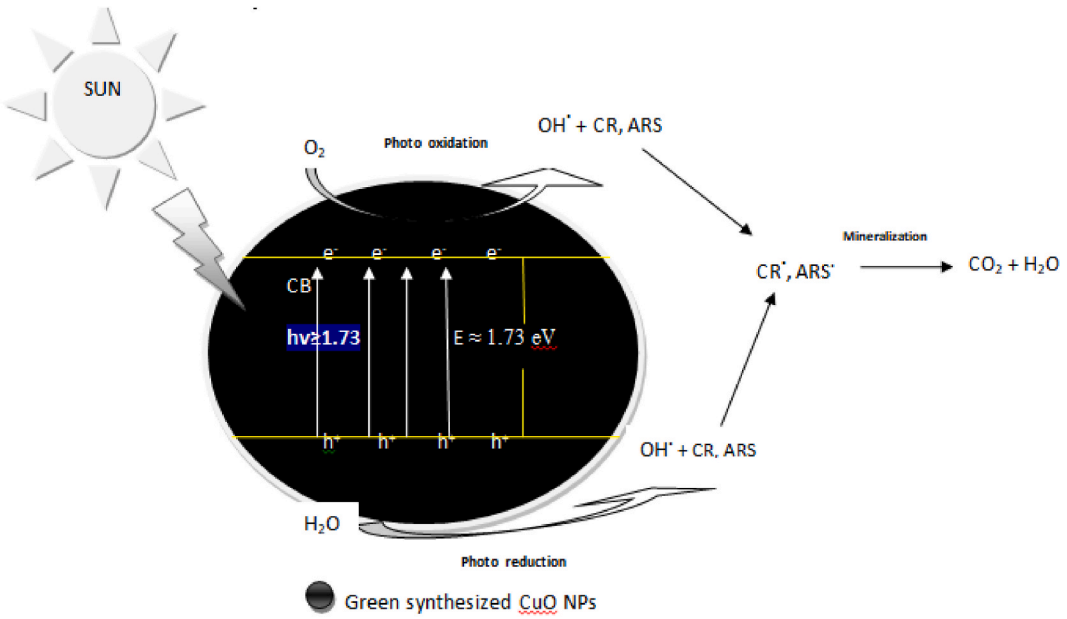

Fig. 11. Proposed mechanism of photocatalytic degradation for Congo red and Alizarin red S. (For interpretation of the references to color in this figure legend, the reader is referred to the Web version of this article.)

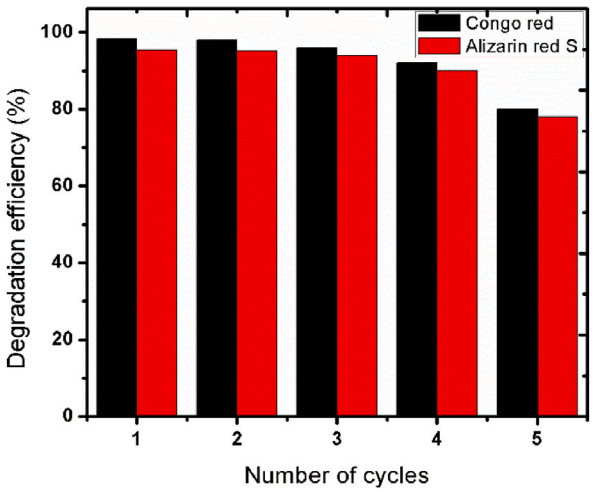

Fig. 12. Recyclability of CuO NPs at optimum experimental parameters

Data availability statement

Data will be made available on request.

Funding

This work was funded by Dilla University.

Declaration of competing interest

The authors declare that they have no known competing financial interests or personal relationships that could have appeared to influence the work reported in this paper.

Table 1
Comparison of green synthesized CuO NPs in degradation efficiency and particle size with reported values.

Developed material	Reducing and capping agent	Particle size (nm)	Targeted pollutant	Reagent added to trigger degradation	Utilised light	Degradation efficiency (%)	Reference
CuO NPs	*Moringa stenopetala* seed extract	6.556	Congo red, Alizarin red S	_	Solar light	98.35 and 95.4 respectively	This work
	Cordia sebestena flower extract	20 to 35	Bromothymol blue	H_2O_2	Solar light	100	[45]
	Papaya Peel Extract	85–140	palm oil mill effluent	_	UV light	66	[57]
	Carica papayaleaves extract	140	Coomassie brilliant blue	–	Solar light	_	[47]
	Psidium guajava leaf	–	Nile blue, reactive yellow	_	Solar light	97 and 80 respectively	[33]
	Oak Fruit Hull extract	40	Basic violet 3	–	fluorescent lamp (visible light)	86	[58]

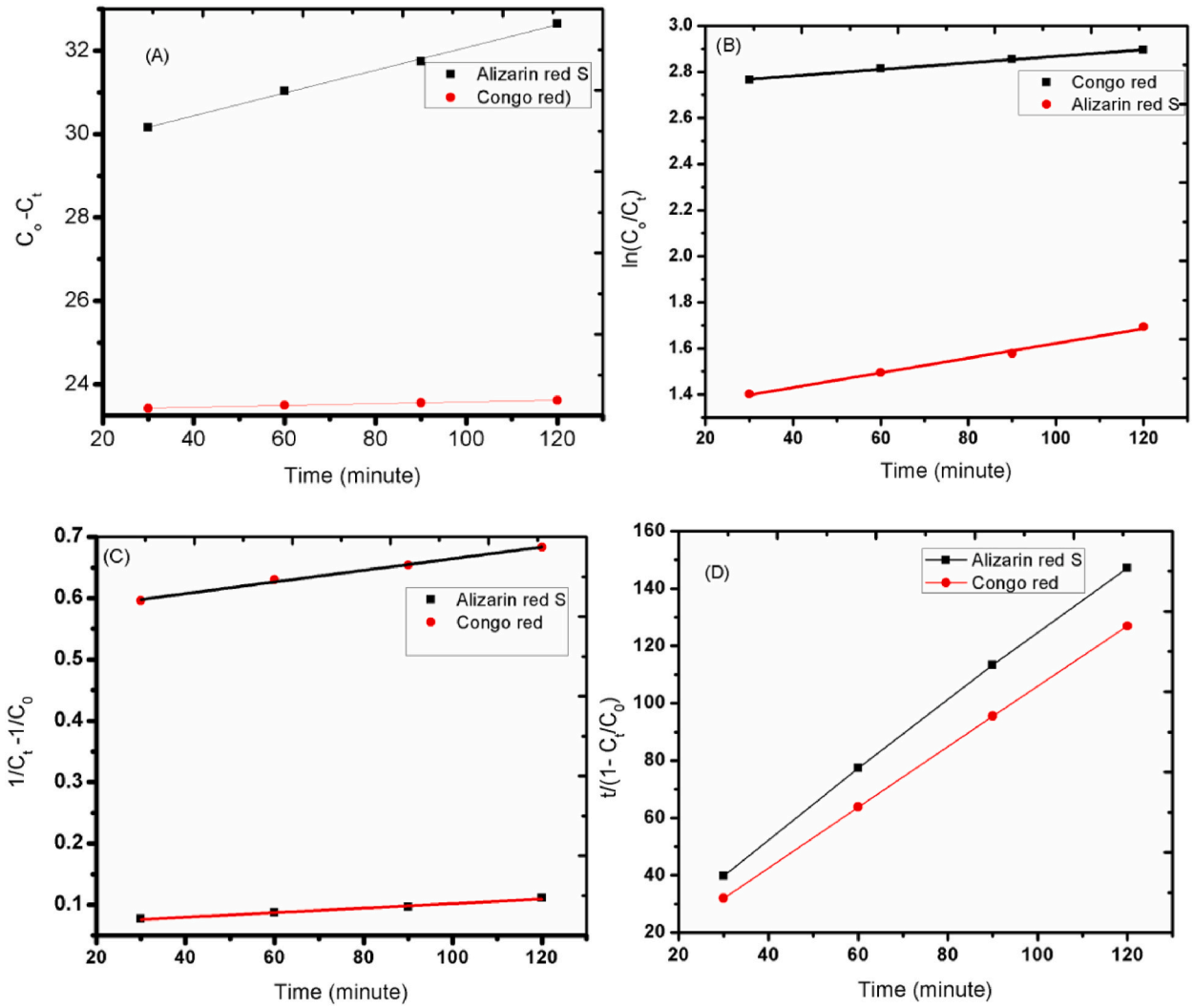

Fig. 13. Pseudo zero-order (A), first order (B), second order (C), and MBG (D) kinetic model for Alizarin red S and Congo red degradation. (For interpretation of the references to color in this figure legend, the reader is referred to the Web version of this article.)

Table 2
Rate constant (k) or 1/m and correlation coefficient (R^2) calculated for kinetics model.

Types of models	Dyes			
	Alizarin red S.		Congo red	
	k ($\frac{1}{m}$ for BMG)	R^2	k ($\frac{1}{m}$ for BMG)	R^2
Pseudo zero order	0.0273	0.997	0.0021	0.995
Pseudo first order	0.0032	0.9927	0.00142	0.997
Pseudo second order	0.00037	0.980	0.00095	0.993
BMG model	1.1929	0.9991	1.0549	0.99999

Acknowledgements

The authors acknowledge Dilla University and Hawassa University for the financial and material support for this work.

References

[1] O. Sacco, et al., Photocatalytic degradation of organic dyes under visible light on N-doped TiO_2 photocatalysts, Int. J. Photoenergy 2012 (2012).
[2] P. Falcaro, et al., Application of metal and metal oxide nanoparticles@ MOFs, Coord. Chem. Rev. 307 (2016) 237–254.
[3] J.W. Rasmussen, et al., Zinc oxide nanoparticles for selective destruction of tumor cells and potential for drug delivery applications, Expet Opin. Drug Deliv. 7 (9) (2010) 1063–1077.
[4] M.B. Gawande, et al., Cu and Cu-based nanoparticles: synthesis and applications in catalysis, Chem. Rev. 116 (6) (2016) 3722–3811.
[5] A.A. Umar, M. Oyama, A seed-mediated growth method for vertical array of single-crystalline CuO nanowires on surfaces, Cryst. Growth Des. 7 (12) (2007) 2404–2409.
[6] N. Pavithra, et al., Combustion-derived CuO nanoparticles: application studies on lithium-ion battery and photocatalytic activities, Inorg. Chem. Commun. 130 (2021), 108689.
[7] S. Surendhiran, et al., Rapid green synthesis of CuO nanoparticles and evaluation of its photocatalytic and electrochemical corrosion inhibition performance, Mater. Today: Proc.47(4) (2021) 1011–1016.
[8] H. Harini, G. Nagaraju, B. Nirmala, Combustion synthesis CuO nanoparticles: application to photocatalytic activity, Mater. Today: Proc. 49 (3) (2021) 860–864.
[9] M.B. Zaman, et al., Biogenic synthesis of CuO nanoparticles using Tamarindus indica L. and a study of their photocatalytic and antibacterial activity, Environ. Nanotechnol. Monit. Manag. 14 (2020), 100346.
[10] A. Sharma, et al., Facile synthesis, physico-chemical studies of Ocimum sanctum magnetic nanocomposite and its adsorptive application against Methylene blue, J. Mol. Liq. 362 (2022), 119752.
[11] M. Ghalkhani, et al., Green synthesis of nonprecious metal-doped copper hydroxide nanoparticles for construction of a dopamine sensor, Future Med. Chem. 13 (8) (2021) 715–729.
[12] S. Naraginti, et al., *Enhanced photo-catalytic activity of Sr and Ag co-doped TiO_2 nanoparticles for the degradation of Direct Green-6 and Reactive Blue-160 under UV & visible light*, Spectrochim. Acta Mol. Biomol. Spectrosc. 149 (2015) 571–579.
[13] M.A. Hassaan, A. El Nemr, A. Hassaan, Health and environmental impacts of dyes: mini review, Am. J. Environ. Sci. Eng. 1 (3) (2017) 64–67.
[14] A.A. Alqadami, et al., Adsorptive performance of MOF nanocomposite for methylene blue and malachite green dyes: kinetics, isotherm and mechanism, J. Environ. Manag. 223 (2018) 29–36.
[15] A.A. Alqadami, et al., *Adsorptive removal of toxic dye using Fe_3O_4–TSC nanocomposite: equilibrium, kinetic, and thermodynamic studies*, J. Chem. Eng. Data 61 (11) (2016) 3806–3813.
[16] T. Tatarchuk, et al., Adsorptive removal of toxic Methylene Blue and Acid Orange 7 dyes from aqueous medium using cobalt-zinc ferrite nanoadsorbents, Desalination Water Treat. 150 (2019) 374–385.
[17] E. Daneshvar, et al., Desorption of methylene blue dye from brown macroalga: effects of operating parameters, isotherm study and kinetic modeling, J. Clean. Prod. 152 (2017) 443–453.
[18] A. Sharma, D. Mangla, S.A. Chaudhry, Recent advances in magnetic composites as adsorbents for wastewater remediation, J. Environ. Manag. 306 (2022), 114483.
[19] A. Choudhry, et al., Origanum vulgare manganese ferrite nanocomposite: an advanced multifunctional hybrid material for dye remediation, Environ. Res. 220 (2023), 115193.
[20] H. Kaur, et al., A novel and one-pot synthesis of Punica granatum mediated copper oxide having flower-like morphology as an efficient visible-light driven photocatalyst for degradation of textile dyes in waste water, J. Mol. Liq. 355 (2022), 118966.
[21] N.J. Vickers, Animal communication: when i'm calling you, will you answer too? Curr. Biol. 27 (14) (2017) R713–R715.
[22] E.E. Ebrahiem, M.N. Al-Maghrabi, A.R. Mobarki, Removal of organic pollutants from industrial wastewater by applying photo-Fenton oxidation technology, Arab. J. Chem. 10 (2017) S1674–S1679.
[23] D. Kang, et al., Novel Al-doped carbon nanotubes with adsorption and coagulation promotion for organic pollutant removal, J. Environ. Sci. 54 (2017) 1–12.
[24] B.E. Barragán, C. Costa, M.C. Marquez, Biodegradation of azo dyes by bacteria inoculated on solid media, Dyes Pigments 75 (1) (2007) 73–81.
[25] V. Ashouri, et al., Synthesis and shaping of Zr-UiO-66 MOF applicable as efficient phosalone adsorbent in real samples, Polyhedron 215 (2022), 115653.
[26] V. Ashouri, et al., Preparation of the extruded UiO-66-based Metal-Organic Framework for the diazinon removal from the real samples, J. Mol. Struct. 1240 (2021), 130607.
[27] M. Ghalkhani, H. Charkhan, M. Sabbaghan, *Synthesis and application of a powerful heterogeneous photo-Fenton catalyst based on rGO/g-C_3N_4/Fe_3O_4/tiO_2 nano-composite for the removal of sewage contaminants*, J. Electrochem. Soc. 167 (6) (2020), 067515.
[28] L.H. Shindume, et al., *Enhanced photocatalytic activity of B, N-codoped TiO_2 by a new molten nitrate process*, J. Nanosci. Nanotechnol. 19 (2) (2019) 839–849.
[29] D. Pan, et al., Synthesis, characterization and photocatalytic activity of mixed-metal oxides derived from NiCoFe ternary layered double hydroxides, Dalton Trans. 47 (29) (2018) 9765–9778.
[30] B. Zhao, et al., Yeast-template synthesized Fe-doped cerium oxide hollow microspheres for visible photodegradation of acid orange 7, J. Colloid Interface Sci. 511 (2018) 39–47.
[31] A. Aslam, et al., Kinetics of acid blue 40 dye degradation under solar light in the presence of CuO nanoparticles synthesized using Citrullus lanatus seeds extract, Z. Phys. Chem. 236 (4) (2022) 583–594.
[32] J. Akter, et al., *Kinetically controlled selective synthesis of Cu_2O and CuO nanoparticles toward enhanced degradation of methylene blue using ultraviolet and sun light*, Mater. Sci. Semicond. Process. 123 (2021), 105570.
[33] J. Singh, et al., Biogenic synthesis of copper oxide nanoparticles using plant extract and its prodigious potential for photocatalytic degradation of dyes, Environ. Res. 177 (2019), 108569.

[34] F. Khan, et al., Degradation of persistent organic pollutant using Ag-doped ZnO-ZnS–polyaniline composite as photocatalyst, Int. J. Environ. Sci. Technol. (2022) 1–16.
[35] M. Rahmat, et al., *Bionanocomposite of Au decorated MnO_2 via in situ green synthesis route and antimicrobial activity evaluation*, Arab. J. Chem. 14 (12) (2021), 103415.
[36] J.K. Sharma, et al., Green synthesis of CuO nanoparticles with leaf extract of Calotropis gigantea and its dye-sensitized solar cells applications, J. Alloys Compd. 632 (2015) 321–325.
[37] J. Singh, et al., 'Green'synthesis of metals and their oxide nanoparticles: applications for environmental remediation, J. Nanobiotechnol. 16 (1) (2018) 1–24.
[38] S. Yasmin, et al., Green synthesis, characterization and photocatalytic applications of silver nanoparticles using Diospyros lotus, Green Process. Synth. 9 (1) (2020) 87–96.
[39] F. Gebregiorgis, T. Negesse, A. Nurfeta, Feed intake and utilization in sheep fed graded levels of dried moringa (Moringa stenopetala) leaf as a supplement to Rhodes grass hay, Trop. Anim. Health Prod. 44 (3) (2012) 511–517.
[40] A. Ejigu, et al., Moringa stenopetala seed oil as a potential feedstock for biodiesel production in Ethiopia, Green Chem. 12 (2) (2010) 316–320.
[41] L. Adane, M. Teshome, Y. Tariku, Isolation of compounds from root bark extracts of Moringa stenopetala and evaluation of their antibacterial activities, J. Pharmacogn. Phytochem. 8 (3) (2019) 4228–4244.
[42] C. Metsopkeng, et al., Comparative study of Moringa stenopetala root and leaf extracts against the bacteria Staphyloccocus aureus strain from aquatic environment, Scient. Afr. 10 (2020), e00549.
[43] Y. Mekonnen, B. Dräger, Glucosinolates in moringa stenopetala, Planta Med. 69 (4) (2003) 380–382.
[44] E. Nibret, M. Wink, Trypanocidal and antileukaemic effects of the essential oils of Hagenia abyssinica, Leonotis ocymifolia, Moringa stenopetala, and their main individual constituents, Phytomedicine 17 (12) (2010) 911–920.
[45] S. Prakash, et al., Green synthesis of copper oxide nanoparticles and its effective applications in Biginelli reaction, BTB photodegradation and antibacterial activity, Adv. Powder Technol. 29 (12) (2018) 3315–3326.
[46] P.K. Raul, et al., CuO nanorods: a potential and efficient adsorbent in water purification, RSC Adv. 4 (76) (2014) 40580–40587.
[47] R. Sankar, et al., Green synthesis of colloidal copper oxide nanoparticles using Carica papaya and its application in photocatalytic dye degradation, Spectrochim. Acta Mol. Biomol. Spectrosc. 121 (2014) 746–750.
[48] A. Kassim, et al., Preparation and characterization of iron sulphide thin films by chemical bath deposition method, Indon. J. Chem. 10 (1) (2010) 8–11.
[49] L. Debbichi, et al., *Vibrational properties of CuO and Cu_4O_3 from first-principles calculations, and Raman and infrared spectroscopy*, J. Phys. Chem. C 116 (18) (2012) 10232–10237.
[50] F. Mai, et al., Mechanisms of photocatalytic degradation of Victoria Blue R using nano-TiO2, Separ. Purif. Technol. 62 (2) (2008) 423–436.
[51] P.K. Boruah, et al., *Sunlight assisted degradation of dye molecules and reduction of toxic Cr (VI) in aqueous medium using magnetically recoverable Fe_3O_4/reduced graphene oxide nanocomposite*, RSC Adv. 6 (13) (2016) 11049–11063.
[52] S. Sohrabnezhad, A. Pourahmad, E. Radaee, Photocatalytic degradation of basic blue 9 by CoS nanoparticles supported on AlMCM-41 material as a catalyst, J. Hazard Mater. 170 (1) (2009) 184–190.
[53] N. Venkatachalam, et al., *Enhanced photocatalytic degradation of 4-chlorophenol by Zr^{4+} doped nano TiO_2*, J. Mol. Catal. Chem. 266 (1–2) (2007) 158–165.
[54] F. Kiriakidou, D.I. Kondarides, X.E. Verykios, *The effect of operational parameters and TiO_2-doping on the photocatalytic degradation of azo-dyes*, Catal. Today 54 (1) (1999) 119–130.
[55] W. Nam, J. Kim, G. Han, Photocatalytic oxidation of methyl orange in a three-phase fluidized bed reactor, Chemosphere 47 (9) (2002) 1019–1024.
[56] P. Faria, J. Orfao, M. Pereira, Adsorption of anionic and cationic dyes on activated carbons with different surface chemistries, Water Res. 38 (8) (2004) 2043–2052.
[57] Y.-K. Phang, et al., Green synthesis and characterization of CuO nanoparticles derived from papaya peel extract for the photocatalytic degradation of palm oil mill effluent (POME), Sustainability 13 (2) (2021) 796.
[58] M. Sorbiun, et al., Green synthesis of zinc oxide and copper oxide nanoparticles using aqueous extract of oak fruit hull (jaft) and comparing their photocatalytic degradation of basic violet 3, Int. J. Environ. Res. 12 (1) (2018) 29–37.